

# 1 Elucidating loessal landslide initiation in wood- and shrub-land by hydro-mechanical 2 heterogeneity

3 Ruijie Yang, Chao Ma, Xi Yang, Yan Zhang, Liqun Lyu, Xinying Wang

4 School of Soil and Water Conservation, Beijing Forestry University, Beijing 100083, PR China

5 Corresponding author: Professor Chao Ma, sanguoxumei@163.com

6 **Abstract:** Vegetation recovery on the Chinese Loess Plateau has markedly changed the hydrological and mechanical  
7 controls on hillslope erosion, shifting sediment production from runoff-driven erosion to gravity-driven processes  
8 such as rainfall-induced loessal landslides. Presently, few studies have clearly documented the differences in  
9 landslide erosion and initiation between shrubland and woodland. We conducted field investigations, rainfall soil-  
10 moisture observations, dye-tracer experiments, and soil-root tests, to examine landslide characteristics in terms of  
11 geometry and volume, excess soil-water ratio, preferential-flow pathways, and failure potential in the two stands.  
12 Rainfall-induced loessal landslides in the shrubland stand have shallower failure depths and smaller volumes but are  
13 wider than those in the woodland stand, and they are triggered under lower contributing area-slope conditions.  
14 Moreover, vertical infiltration in the woodland stand tends to be more stable and efficient, characterized by greater  
15 water penetration depth and enhanced pore connectivity. The relationship between the excess soil-water ratio and  
16 soil-water storage demonstrates that subsurface flow in woodland stand is triggered at relatively lower degrees of  
17 saturation. This behavior is attributed to well-developed preferential-flow pathways and reduced matric suction. The  
18 landscape dissection-rainfall index indicates lower landslide susceptibility on steep woodland slopes than on steep  
19 shrubland slopes, consistent with the lower landslide density in woodland relative to shrubland. Overall, these  
20 hydrological and mechanical contrasts indicate that woodland slopes, by combining deep root systems, stable  
21 preferential-flow pathways, and strong mechanical reinforcement, support an effective subsurface flow system that  
22 enhances infiltration and delays shallow saturation, thus improving slope stability. These results highlight the need  
23 to reassess sediment production on the Loess Plateau by explicitly accounting for landslides rather than attributing  
24 it solely to runoff-driven erosion.

25 **Keywords:** Shallow landslide; Hillslope hydrology; Landscape dissection-rainfall index

## 26 1 Introduction

27 The Chinese Loess Plateau is one of the most erosive landscapes in the world (Fu et al., 2016; Borrelli et al.,  
28 2020; Bai et al., 2024). Since 1980, ecological rehabilitation has significantly improved regional vegetation cover  
29 and structure, with vegetation cover now reaching approximately 60% (Feng et al., 2016; Deng et al., 2022; Liao et  
30 al., 2025). Restored vegetation, optimized plant community structure, and surface litter accumulation have enhanced  
31 water storage capacity and slope stability (Yan et al., 2024; Liu et al., 2025). Since 2010, the region has experienced  
32 several rainstorms that are unprecedented in the historical record, as exemplified by storms in 2013, 2017, and 2025  
33 (Tang et al., 2020; Deng et al., 2022; Yang et al., 2023; Hao et al., 2024). Subsequent studies have reported a shift  
34 in the dominant erosion process from dispersed runoff erosion to gravitational mass movements (Yang et al., 2024;  
35 Du et al., 2025). These findings sufficiently indicate that vegetation recovery on Chinese Loess Plateau alters the  
36 dominant sediment-producing processes and soil-erosion patterns.

37 Vegetation recovery can enhance ecosystem functioning and alter the rainwater infiltration pathways (Gu et al.,  
38 2019; Wang et al., 2022; Guan et al., 2024). Increases in surface cover and root penetration significantly enhance  
39 rainfall infiltration and promote greater spatial heterogeneity, non-uniform infiltration patterns, and preferential-flow  
40 pathways (Li et al., 2007; Zhao et al., 2022). Preferential flow often serves as a primary pathway for rainfall  
41 infiltration and can bypass soil-matrix pores to reach deeper soil layers (Bachmair et al., 2012; Franklin et al., 2021).

42 Preferential flow intensity and morphology vary markedly among vegetation types. Woodland slopes are  
43 characterized by deep, continuous macropore channels, predominantly vertical preferential flow, rapid infiltration,  
44 and greater deep-soil water storage (Niu et al., 2023; Cai et al., 2024; Zhang et al., 2025). Shrubland slopes exhibit  
45 predominantly lateral and diffuse subsurface flow with weak vertical components, thereby retaining much of the  
46 infiltrating water in shallow soil layers (Wang et al., 2020; An et al., 2022; Liang et al., 2023; Zhang et al., 2024).  
47 Herbaceous slopes rely mainly on surface cracks and earthworm burrows to route water, and therefore preferential  
48 flow channels are sparse and discontinuous (Wen et al., 2020; Niu et al., 2023; Li et al., 2025). Vegetation recovery  
49 has significantly restructured the soil bio-pore system through root penetration, thereby facilitating the development  
50 of preferential-flow pathways and making infiltration regimes more heterogeneous (Zhao et al., 2022; Guan et al.,  
51 2024). However, preferential-flow infiltration on steep slopes, particularly at landslide sites with different vegetation  
52 types, has not been adequately investigated. During heavy storms, preferential flow can regulate spatiotemporal  
53 subsurface water dynamics and act as a biologically mediated control on slope stability.

54 Root morphology and spatial configuration influence rainwater infiltration pathways and soil-moisture  
55 redistribution (Fan et al., 2020; Li et al., 2023). On the Chinese Loess Plateau, two predominant vegetation types are  
56 recognized: woodlands dominated by *Robinia pseudoacacia* and *Pinus tabulaeformis*, and shrublands dominated by  
57 *Rosa xanthina* and *Hippophae rhamnoides*. Woodland trees typically develop deeply penetrating root systems,  
58 forming continuous macropore networks and vertical preferential-flow pathways (Zhao et al., 2022; Cai et al., 2024;  
59 Wang and Zhang, 2024). These structures facilitate rapid rainfall infiltration into deep soil layers, enhance subsurface  
60 moisture retention, delay surface saturation, and reduce surface runoff (Souza et al., 2023; Cai et al., 2024; Hu et al.,  
61 2025). In contrast, shrubs develop a dense, fibrous root matrix that promotes mesopores and capillaries formation,  
62 thereby accelerating the formation of subsurface saturation zones and limiting vertical percolation (Laycock et al.,  
63 1967; Souza et al., 2023; Xiao et al., 2024; Yamase et al., 2024). Therefore, plant roots can control preferential-flow  
64 patterns and alter hillslope hydrology. However, few studies have examined how the hydrological effects of mature  
65 vegetation influence landslides on the Chinese Loess Plateau.

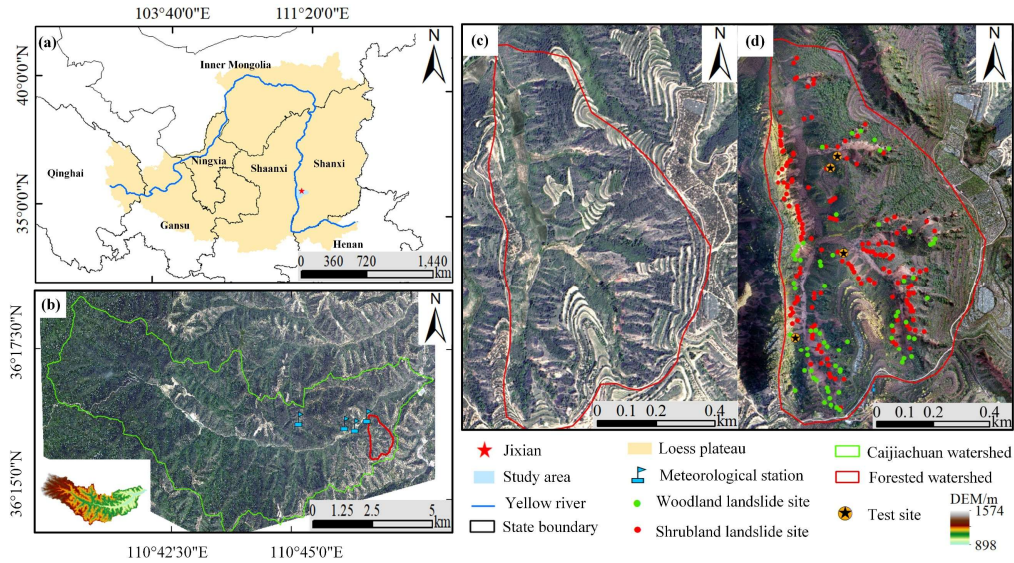
66 To examine the hydrological and mechanical heterogeneity in mature woodland and shrubland stands on steep  
67 slopes and its implications for slope stability, we first analyze landslide geometry and landscape dissection for slides  
68 triggered by a low-intensity storm from 3 to 6 October 2021. Then, we assess hydrological heterogeneity in mature  
69 woodland and shrubland using soil-moisture observations, excess soil-water ratios across different soil-water storage  
70 levels, and preferential-flow pathway identification. Mechanical heterogeneity is characterized by soil and root  
71 strength parameters, the soil water characteristic curve (SWCC), and the hydraulic conductivity function (HCF).  
72 Finally, we evaluate slope failure potential in relation to landslide density in the two stands. This study mainly  
73 addresses the role of vegetation in modulating slope stability by analyzing real landslide cases. Our findings highlight  
74 the dual role of vegetation in mitigating landslide erosion and provide new insights into its nuanced effects on  
75 hillslope stability.

## 76 **2. Research background**

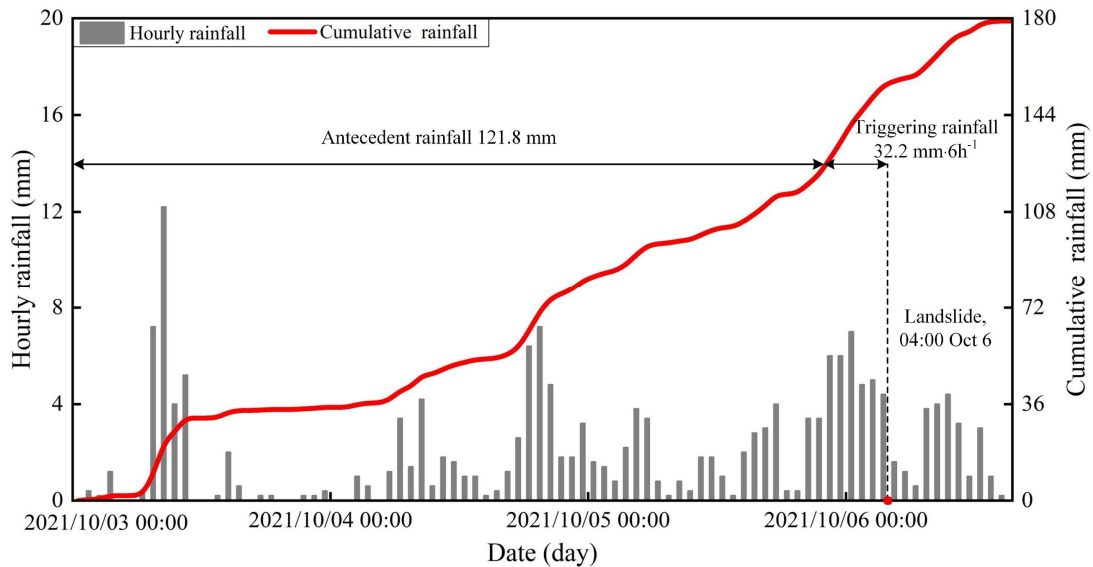
### 77 **2.1 Study area**

78 The study area lies in a forested catchment on the southeastern Loess Plateau in China (Fig. 1a). It is located in  
79 the downstream reach of the Caijiachuan watershed in Jixian County, Shanxi Province (Fig. 1b). The soil has an  
80 unconsolidated, porous structure. On steep slopes, woodland is dominated by *Robinia pseudoacacia* and shrubland  
81 by *Rosa xanthina*. Since the farmland reforestation policy was implemented in 1980, forest cover has recovered to  
82 about 70%. During 1990–1995 and 1999–2002, the Mountain Improvement Technology Training Project enhanced  
83 forest regeneration. Currently, the local soil and water conservation measures serve as a benchmark within the Loess

84 Plateau region. The area has four distinctive seasons and a cold semi-arid climate . The annual precipitation is  
 85 approximately 579.1 mm, and the mean annual temperature is 9.9°C. Most rain events occurs from June to September,  
 86 accounting for more than 70% of the annual precipitation. Prior to the 2021 event, a short-duration storm on 25–26  
 87 August 2003 triggered 18 landslides, with antecedent precipitation of 71.7 mm over 18 hours and an intense 3 h  
 88 rainfall of 24.4 mm (Wang et al., 2024). In contrast, the 2021 rainfall event was a low-intensity storm with prolonged  
 89 antecedent precipitation of 121.8 mm over 72 hours and a 6 h peak rainfall of 32.2 mm (Fig. 2). After the storm,  
 90 post-storm documentation mainly focused on differences in landslide numbers, densities, slope aspects, and  
 91 morphological metrics (Tang et al., 2023), while giving little attention to the hydrological and mechanical conditions  
 92 of landslides in the two forested land types.



93  
 94 **Figure 1.** Geographical setting of the study area, with the (a) location of Caijiachuan watershed in the Loess Plateau,  
 95 China, (b) the forested catchment and meteorological stations in downstream reach of Caijiachuan watershed, (c)  
 96 0.15 m resolution orthoimage on 12 October 2019, and (d) 0.10 m resolution orthoimage on 14 October 2021  
 97 showing the sites for soil-moisture observations and dye-tracer experiments.



98  
 99 **Figure 2.** Hourly and cumulative rainfall from 3 to 6 October 2021.

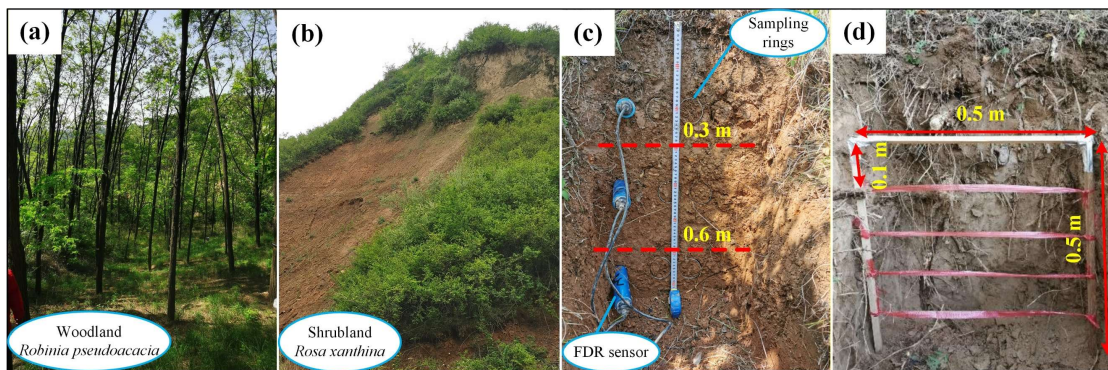
100 **3 Materials and methods**

101 **3.1 Landslide information interpretation**

102 To obtain landslide inventories for the woodland and shrubland, we acquired high-resolution orthoimages and  
103 digital elevation models (DEMs) using an unmanned aerial vehicle (UAV; DJI Inspire 2). Two systematic UAV  
104 flights with consistent flight and image overlap settings were conducted on 12 October 2019 (Fig. 1c) and 14 October  
105 2021 (Fig. 1d). Pix4Dmapper (version 4.6, Pix4D SA, Switzerland) was used to generate ortho-mosaics and DEMs.  
106 These DEMs have spatial resolutions of 0.15 m and 0.10 m, respectively, thereby supporting accurate landslide  
107 mapping. Landslide point and areal densities are calculated by dividing the total number of landslides and the total  
108 scar area by the woodland and shrubland areas, respectively. The lateral extent of each landslide is the sum of the  
109 sidewall and head scarp areas. The unit upslope contribution area is the ratio of the total contributing area to the scar  
110 width. Slope gradients and associated unit contributing areas are computed from the DEM generated on 14 October  
111 2021.

112 **3.2 Rainfall, soil-moisture monitoring and sample collection**

113 In the study area, the woodland has an open structure due to sparse-to-moderate tree density and high canopy  
114 height (Fig. 3a), whereas the shrubland has a closed structure because of high density and low canopy height (Fig.  
115 3b). Each study site is dominated by single woody species, with *Robinia pseudoacacia* in the woodland and *Rosa*  
116 *xanthina* in the shrubland. Both land types have a well-developed herbaceous layer. To investigate the hillslope  
117 hydrology, we used frequency-domain reflectometry (FDR) soil-moisture sensors installed at depths of 30, 60, and  
118 90 cm to record volumetric water content from May to August 2023 (Fig. 3c). A meteorological station at  
119 Caijiachuan Forest Station is approximately 2 kilometers to the northwest of the study area. During soil-moisture  
120 sensor installation, we collected undisturbed soil samples near the FDR sensor locations. Bulk density, porosity,  
121 effective cohesion, internal friction angle, and unsaturated hydraulic properties were determined using an electronic  
122 balance, an oven, a GDS triaxial apparatus, and transient release and imbibition tests (Lu and Godt, 2013). Plant  
123 roots were collected to determine depth-dependent root distribution (Fig. 3d), root diameter, root area ratio, and  
124 tensile strength (Nimmo et al., 2009).



125 **Figure 3.** Soil moisture monitoring and soil and root sampling. (a) Open woodland dominated by *Robinia*  
126 *pseudoacacia*. (b) Close-structure shrubland dominated by *Rosa xanthina*. (c) Trench wall showing soil sampling  
127 and FDR sensor installation. (d) In situ root counting and sampling at 0.1 m depth intervals.  
128

129 **3.3 Excessive soil water due to preferential flow**

130 Previous studies of preferential flow on the Loess Plateau have shown that continuous channels in woodland  
131 enhance deep soil water storage, whereas lateral and dispersed channels in shrubland keep water in shallow soil  
132 layers (Wang et al., 2019; An et al., 2022). Therefore, differences in preferential-flow pathways can result in distinct  
133 soil-moisture responses during the same rainfall event. In this study, we first characterized preferential-flow

134 pathways using dye tracer experiments and then examined soil-moisture responses using observed soil-moisture data.

135 Dye tracer experiments were conducted on vegetated slopes near the soil-moisture monitoring sites to examine  
136 the preferential flow pathways (Fig. 1d). The slope angles were 35.8° at the woodland site and 38.2° at the shrubland  
137 site. An electric sprayer was used to spray a 4 g·L<sup>-1</sup> brilliant blue solution onto a 100 cm × 100 cm plot (Figs. 4a and  
138 4b). After spraying the solution, the plot was immediately covered with a rainproof cloth to minimize evaporation.  
139 After 24 h, a 5 cm-wide margin of soil was removed from the plot edges, and the core area was excavated to obtain  
140 10 vertical and 5 horizontal profiles. Excavation grids were established at 0.1 m intervals in both the longitudinal  
141 and transverse directions (Figs. 4c and 4d). Profile images were captured with a digital camera at a fixed distance  
142 and in a parallel orientation, and subsequently processed using Adobe Photoshop (version 2021; Adobe Inc., USA)  
143 and Image-Pro Plus (version 6.0; Media Cybernetics, USA). The proportion of flow marked by the dye is:

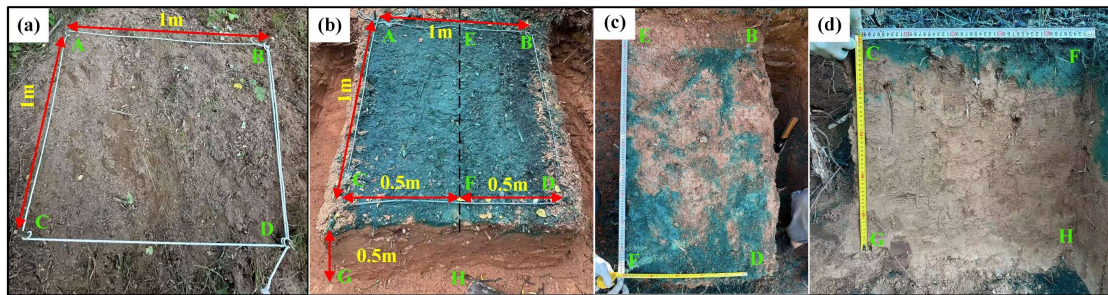
$$144 \quad SAR = \frac{a_j}{A_j} \quad (1)$$

145 where  $SAR$  is the stained-area ratio for the soil profile,  $j$  is soil depth (cm),  $a$  is the number of stained pixels at  
146 depth  $j$ , and  $A$  is the total number of pixels along the image width at depth  $j$ .

147 The soil-moisture response index describes excess soil water in response to a given rainfall input:

$$148 \quad R_C = \frac{R_{max} - (R + R_0)}{R + R_0} \quad (2)$$

149 where  $R_C$  is the excess soil-water ratio in response to a given rainfall event,  $R_{max}$  is the maximum total soil-water  
150 storage during the rainfall episode (mm),  $R$  is the cumulative rainfall during the episode (mm), and  $R_0$  is the initial  
151 total soil-water storage before the rainfall episode (mm). Positive or negative values of  $R_C$  indicate whether the  
152 increase in soil-water storage exceeds or falls below the rainfall input. In addition,  $R_C$  reflects the preferential-flow  
153 component aligned with slope orientation or gravity. As soil moisture typically lags rainfall, we follow the method  
154 proposed by Lu et al. (Lu et al., 2024), which defines rainfall episodes using soil depth and in situ saturated hydraulic  
155 conductivity measurements. Therefore, the  $R_C$  values under different  $R + R_0$  conditions, together with the  
156 preferential-flow pathways, can reflect heterogeneity in soil-water movement in the woodland and shrubland.



157  
158 **Figure 4.** Dye tracer experiments and preferential flow pathways examination. (a) Experimental plot after vegetation  
159 removal. (b) Experimental plot after 24 h of brilliant blue solution spraying. (c) Dye-stained profile parallel to the  
160 slope surface. (d) Dye-stained profile along the gravity direction. Capital letters denote corresponding points shared  
161 across Fig. 4 a–d.

### 162 3.4 Slope resistance to failure probability at given rainfall input

163 Hillslope resistance to failure at a given rainfall input depends on the topography and the physical, strength,  
164 and hydraulic properties of soil mass. A widely used combination of the infinite-slope stability model and a  
165 hydrological model yield an expression for the critical drainage area per unit contour length (Montgomery and  
166 Dietrich, 1994):

167 
$$a_{cr} = \frac{zK\sin\theta\cos\theta}{R_t} \left[ \frac{C'+C_r}{\rho_w g z \cos^2 \theta \tan} + \frac{\rho_s}{\rho_w} \left( 1 - \frac{\tan\theta}{\tan\varphi} \right) \right] \quad (3)$$

168 where  $a_{cr}$  is the critical drainage area per unit contour length ( $\text{m}^2 \cdot \text{m}^{-1}$ ),  $R_t$  is the triggering rainfall rate ( $\text{m} \cdot \text{d}^{-1}$ ),  
 169  $K$  is the saturated hydraulic conductivity ( $\text{m} \cdot \text{d}^{-1}$ ),  $\theta$  is the slope angle ( $^\circ$ ),  $C'$  and  $C_r$  are the effective soil  
 170 cohesion and the root-induced cohesion (kPa),  $\rho_s$  and  $\rho_w$  are the unit weights of soil and water ( $\text{KN} \cdot \text{m}^{-3}$ ),  $z$  is  
 171 the soil thickness (m), and  $\varphi$  is the effective internal friction angle ( $^\circ$ ).

172 The left-hand side of Eq. (3) represents the topographic condition of a given landslide or a site susceptible to  
 173 slope failure (Montgomery et al., 2000). Moving  $R$  to the left-hand side yields the right-hand side of Eq. (4) in an  
 174 integrated form involving only soil mass parameters:

175 
$$a_{cr} \times R_t = \frac{K \tan\theta (C' + C_r)}{\rho_w g \tan\varphi} + zK\sin\theta\cos\theta \frac{\rho_s}{\rho_w} \left( 1 - \frac{\tan\theta}{\tan\varphi} \right) \quad (4)$$

176 The physical meaning of  $a_{cr} \times R_t$  is that hillslope resistance to failure under site-specific topographic conditions  
 177 and a given rainfall input strongly depends on soil physical properties. For the rain-induced loessal landslides in the  
 178 study area, the strength and hydraulic properties of the landslide mass in woodland and shrubland may lead to  
 179 different  $a_{cr} \times R_t$  levels, so that landslide density (or number) differs between woodland and shrubland. Therefore,  
 180 we focus on  $a_{cr} \times R_t$  from the right-hand side of Eq. (4) to elucidate the initiation of loessal landslides in two  
 181 forested land types.

## 182 **4 Results**

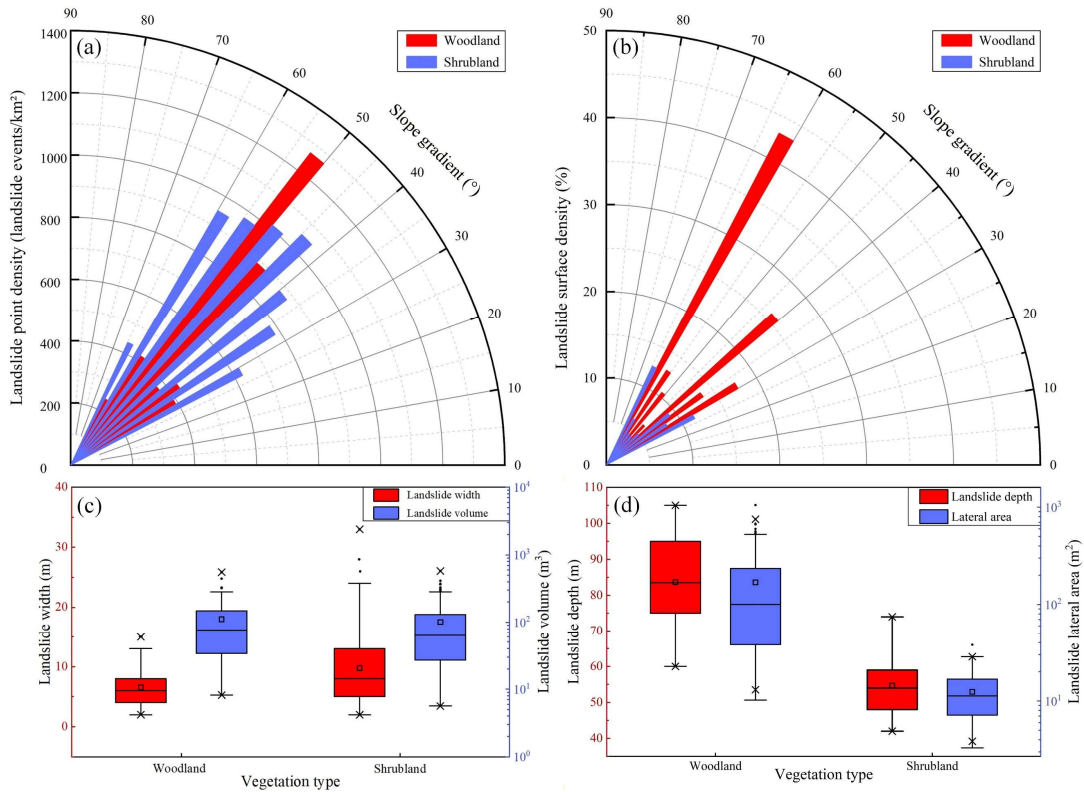
### 183 **4.1 Landslides in the two lands**

184 To compare the landslide point and areal densities between the two stands, we calculated landslide counts and  
 185 areas and divided them by the total steep-terrain area in each stand. This approach excluded non-susceptible terrain  
 186 from the analysis. The spatial distribution and morphology of landslides in woodland and shrubland exhibited clear  
 187 patterns. Specifically, the statistical results showed that landslide point density in shrubland was 1.56 times that in  
 188 woodland, whereas landslide areal density was only 0.48 times that in woodland (Figs. 5a and 5b). Furthermore, the  
 189 average landslide width in shrubland was 1.49 times that in woodland. Generally, trees in woodlands have deep root  
 190 systems that provide stronger anchoring and can mobilize deeper soil layers, thereby modifying the failure depth  
 191 and geometry of shallow landslides (Schwarz et al., 2010; Masi et al., 2023; Dibiagio et al., 2024). The average  
 192 landslide depth in woodland was 1.82 times that in shrubland, while the average lateral extent was 1.61 times that in  
 193 shrubland. However, the average width of landslides in woodland was only 0.67 times that in shrubland. Overall,  
 194 the total landslide volume in woodland was 1.16 times that in shrubland, indicating that landslides in woodland tend  
 195 to be larger (Figs. 5c and 5d).

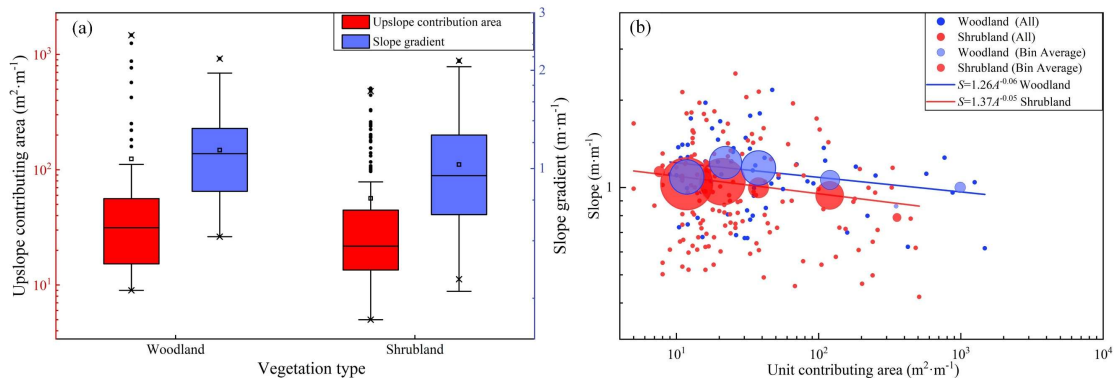
196 When landslides are considered alongside other landscape-dissection agents such as rills and gullies, their  
 197 spatial locations depend on two controls. One is spatial competition between the slope-dependent term  $S = \tan\theta$  ( $\text{m} \cdot \text{m}^{-1}$ )  
 198 and the area-dependent term  $A$  ( $\text{m}^2 \cdot \text{m}^{-1}$ ); the other is exceedance of the  $A$ - $S$  topographic threshold (Montgomery  
 199 and Dietrich, 1994). As highlighted in Sect. 3.4, variations in  $a_{cr} \times R_t$  arise from the interplay of topography, failure  
 200 depth, soil strength, plant root reinforcement, and hydraulic conductivity. To evaluate these controls on landslides,  
 201 we compared the upslope contributing area ( $A$ ) and slope gradient ( $S$ ) between the two land types.

202 Field investigations reveal that most landslides in the study area occur in concave topographic positions.  
 203 Statistical analysis indicates that, on average, woodland sites have a significantly larger upslope contributing area  
 204 ( $124 \text{ m}^2 \text{ m}^{-1}$ ) and steeper slopes ( $48^\circ$ ) than shrubland sites. These values are consistent with expectations from the  
 205  $A$ - $S$  threshold framework (Fig. 6a). Fitting regression lines to the bin-averaged dataset further demonstrates that  
 206 landslides in woodland generally require either a larger upslope contributing area or a steeper slope gradient for

207 initiation (Fig. 6b). The  $A-S$  relationship shows that, at similar slope gradients, landslides in woodland require larger  
 208 upslope contributing areas than those in shrubland. This suggests that, compared with landslides in shrubland, those  
 209 in woodland may require higher rainfall-intensity thresholds, steeper slopes, or both, for initiation. Consistent with  
 210 this, shrubland shows a higher landslide point density than woodland (1.56 times; Fig. 5a).



211 **Figure 5.** Landslide characteristics in woodland and shrubland. **(a)** point density by slope-gradient class; **(b)** areal  
 212 density by slope-gradient class; **(c)** landslide depth and lateral area; and **(d)** landslide width and volume. The three  
 213 horizontal-lines of box show decreasing order of 75th quantile ( $Q_3$ ), median ( $Q_2$ ), and 25th quantile ( $Q_1$ ). The box  
 214 length is the interquartile range ( $IQR=Q_3-Q_1$ ). The small square is the average value. The cross symbols denote the  
 215 1st and 99th percentiles. The upper and lower limit of whiskers are  $Q_3+1.5IQR$  and  $Q_1-1.5IQR$ , respectively. The  
 216 whiskers extend to the most extreme values within these limits; mild outliers are shown as black dots.  
 217



218 **Figure 6.** Upslope contributing area and slope gradient condition. **(a)** upslope contributing area and mean slope as  
 219 a function of slope aspect; **(b)** upslope-contributing area vs. mean slope gradient above the landslide area. The  
 220 definition of the boxplots is given in the caption of Fig. 5. Circles indicate mean slopes, with radius proportional to  
 221 the number of landslides. A power-law regression is fitted to the bin-averaged data.  
 222

## 223 4.2 Soil Hydrological properties

### 224 4.2.1 SWCC and HCF curves

225 Extensive research has examined saturated hydraulic conductivity and microstructural properties of loess (Xu  
226 et al., 2021; Li et al., 2023). Given that loess on hillslopes largely remains unsaturated during natural rainfall  
227 infiltration and drainage (Lan et al., 2021; Wei et al., 2022), evaluating unsaturated hydro-mechanical differences  
228 using SWCCs and HCFs is important. Therefore, this approach enables comparison among key parameters—  
229 hydraulic conductivity, matric suction, suction stress, and microstructural properties.

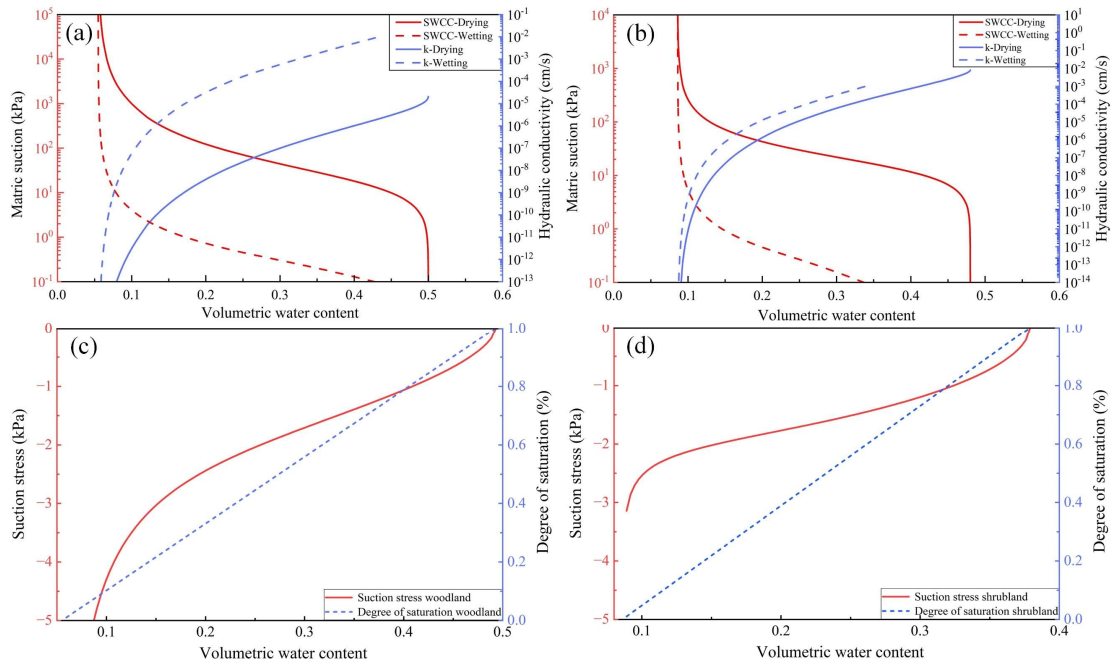
230 Table 1 lists the soil parameters obtained through Hydrus-1D inversion. Based on these parameters, the SWCC  
231 and HCF were plotted for the woodland and shrubland sliding-layer soils (Fig. 7). The results indicate that the pore-  
232 size distribution parameter and saturated hydraulic conductivity are significantly higher for woodland soils than for  
233 shrubland soils. This contrast is evident in both drying and wetting processes. This suggests that the pore system in  
234 woodland soils is dominated by larger pores, which enhance water movement. This pore structure facilitates rainfall  
235 infiltration into the soil. In contrast, shrubland soils contain more micropores that retain more water. This is reflected  
236 in a 3.1% higher residual water content in shrubland soils than in woodland soils. During the drying test, the air-  
237 entry pressures of woodland and shrubland soils are nearly identical. However, during the wetting process, the air-  
238 entry pressure in woodland soils is 0.05 kPa lower than in shrubland soils. This indicates that larger pores in  
239 woodland soils begin to drain and fill with air at lower matric suction. As a result, a continuous gas-phase pathway  
240 forms earlier in woodland soils at the same matric suction (Figs. 7c and 7d). This promotes air-water exchange and  
241 moisture release, making it less likely for the soil to reach or maintain a high degree of saturation for extended  
242 periods. Therefore, under the same rainfall conditions, shrubland soils have weaker moisture-buffering capacity than  
243 woodland soils, making the soil more prone to becoming highly saturated. This reduces the effective stress and shear  
244 strength of shrubland soils, ultimately reducing slope stability.

245 During the drying and wetting processes, the difference in saturated water content in shrubland sliding-layer  
246 soil (0.101) is approximately 14.43 times that in woodland sliding-layer soil (0.007). This indicates that the pore  
247 structure in shrubland sliding-layer soil is less stable than in woodland sliding-layer soil. Under extreme drying-  
248 wetting conditions, some pores tend to collapse or rearrange, making it difficult for the soil to maintain its original  
249 pore configuration. The resulting changes in pore structure disrupt water flow paths in shrubland sliding-layer soil,  
250 reducing permeability, weakening water flow, and slowing drainage. These findings are consistent with the stronger  
251 hysteresis observed in the SWCC of shrubland sliding-layer soil compared with that of woodland sliding-layer soil  
252 (Fig. 7a and 7b). They further confirm that woodland sliding-layer soil has a greater capacity for moisture  
253 redistribution.

254 **Table 1.** Parameters describing the soil and water characteristic curve (SWCC) and the hydraulic conductivity  
255 function (HCF) from Hydrus 1D

Parameters	Definition	Woodland	Shrubland
$\theta_s^d$	Saturated water content	0.500	0.480
$\theta_s^w$		0.493	0.379
$\theta_r$	Residual water content	0.055	0.086
$n^d$	The pore size distribution parameter	1.58	2.19
$n^w$		1.69	1.88
$a^d$ (KPa <sup>-1</sup> )	The inverse of the air entry pressure head	$5.461 \times 10^{-3}$	$6.294 \times 10^{-3}$
$a^w$ (KPa <sup>-1</sup> )		0.646	0.596
$K_s^d$ (cm·s <sup>-1</sup> )	Saturated hydraulic conductivity	$2.3 \times 10^{-5}$	$5.4 \times 10^{-6}$
$K_s^w$ (cm·s <sup>-1</sup> )		$7.1 \times 10^{-2}$	$5.0 \times 10^{-3}$

256 Notes: Superscripts "d" and "w" denote the drying and wetting processes, respectively.

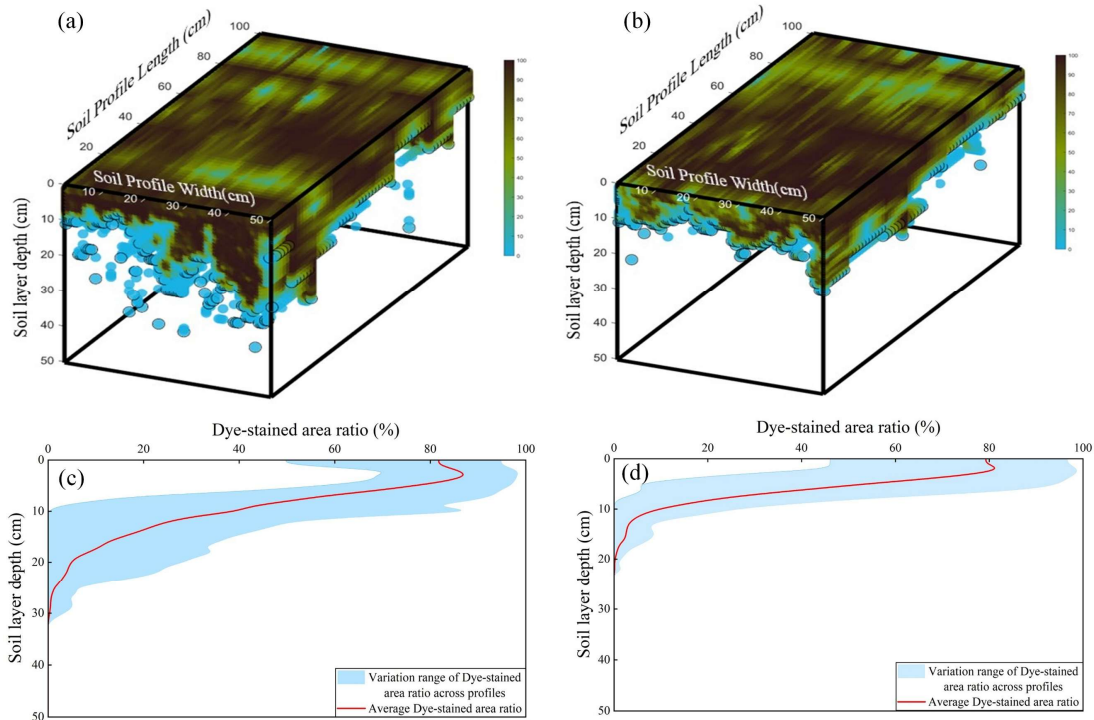


257  
 258 **Figure 7.** Differences in the hydromechanical properties of the sliding-layer soil. **(a)** SWCC for layer 3 of the  
 259 woodland soil profile; **(b)** SWCC for layer 2 of the shrubland soil profile; **(c)** Suction stress–volumetric water content  
 260 curves for layer 3 of the woodland soil profile; **(d)** Suction stress–volumetric water content curves for layer 2 of the  
 261 shrubland soil profile.

262 **4.2.2 Dye tracer experiments**

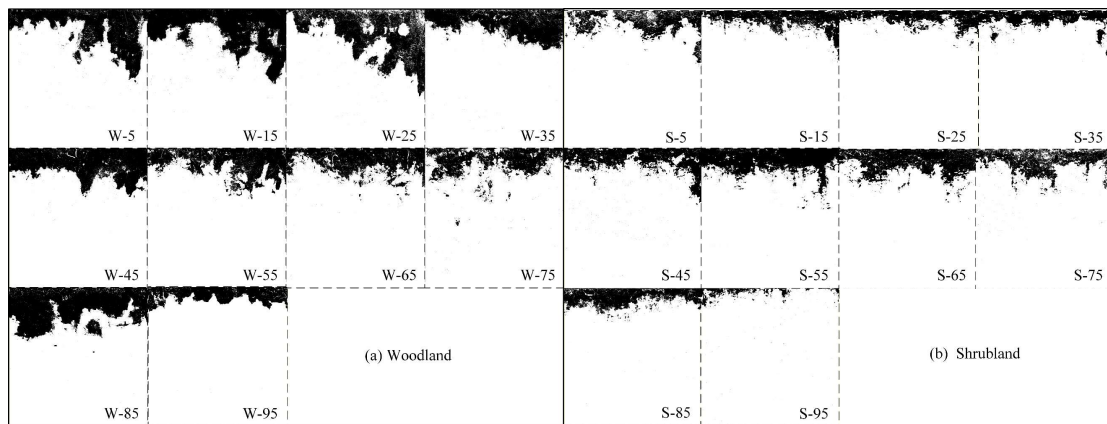
263 Dye-tracer experiments directly visualize the flow pathways of water infiltration in woodland and shrubland  
 264 soils. Under the same applied water volume and infiltration area, the stained soil volume in woodland soils is  
 265 markedly larger than that in shrubland soils. Three-dimensional visualizations reveal that stained pathways in  
 266 woodland soils form thick bands with numerous vertically continuous columnar channels. Hydraulic connectivity is  
 267 high, and water infiltrates to greater depths. Stained bands in shrubland soils are shallow, and vertical, filament-like  
 268 channels are nearly absent. In addition, the depth-dependent pattern of dye-stained area ratios in the shrubland profile  
 269 further confirms that vertical infiltration is restricted to relatively shallow depths. Differences in the volume, depth,  
 270 and morphology of the stained pathways indicate that infiltration in woodland soils no longer follows uniform  
 271 matrix-flow conditions. This is also evident in the dye-stained areas of vertical profiles. Woodland profiles show  
 272 large, continuous color patches, whereas shrubland profiles mainly show fragmented spots concentrated in shallow  
 273 soil. This pattern suggests that deeper shrubland soils are denser and have lower pore connectivity.

274 Overall, woodland soils more readily develop a stable, efficient vertical percolation system with greater  
 275 infiltration depth and stronger connectivity. This promotes deep water storage and redistribution. In contrast,  
 276 insufficient pore connectivity in shrubland soils causes water to remain in shallow layers, prolonging surface wetness  
 277 and slowing pore-water pressure recovery. Under intense rainfall, this condition favors saturation buildup and thus  
 278 increases the likelihood of landslide initiation. This flow pattern is consistent with the SWCC- and HCF-inferred  
 279 differences in soil hydraulic behavior and provides direct, pathway-scale evidence of flow pathways, which cannot  
 280 be resolved from the curve-derived hydraulic parameters alone.



281

282 **Figure 8.** Morphological characteristics of dye-stained flow paths in woodland and shrubland soils. **(a)** Three-  
 283 dimensional visualization of stained zones in woodland; **(b)** Three-dimensional visualization of stained zones in  
 284 shrubland; **(c)** Dye-stained area ratio vs. soil depth in woodland; **(d)** Dye-stained area ratio vs. soil depth in shrubland.

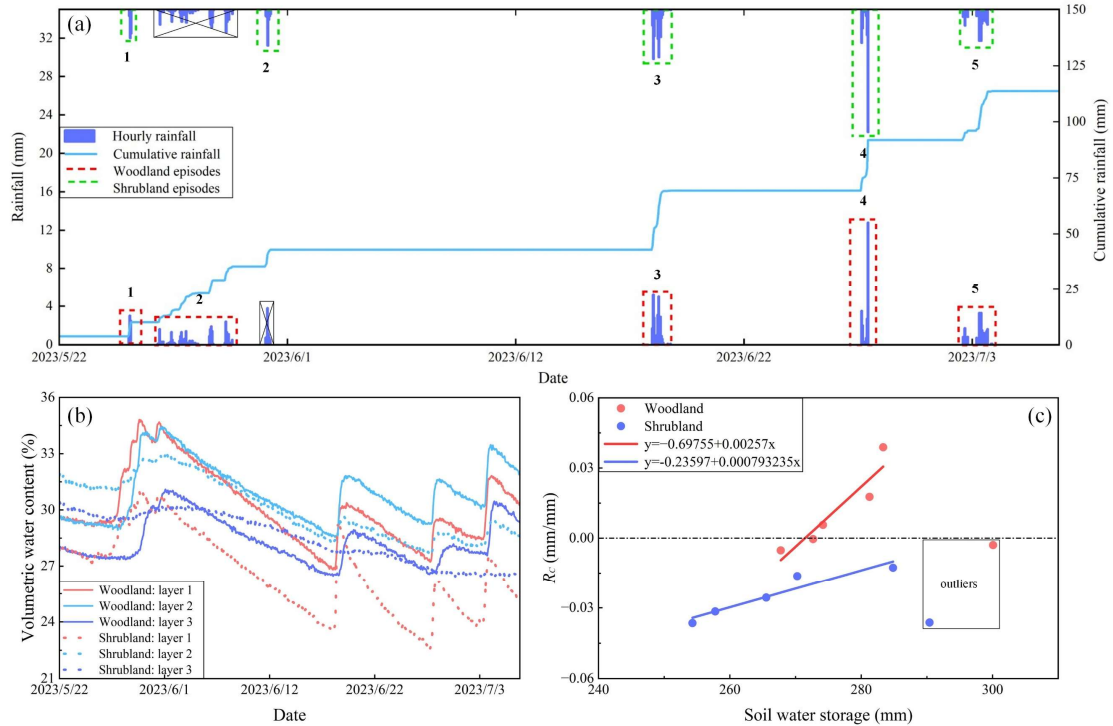


285

286 **Figure 9.** Schematic dye-stained vertical soil profiles at different hillslope positions. **(a)** Woodland profile; **(b)**  
 287 Shrubland profile. Numbers from 0 to 100 denote relative slope positions, with lower values indicating locations  
 288 near the slope base.

289 **4.3 Slope hydrological characteristics**

290 To characterize how woodland and shrubland soils respond to rainfall, we group rainfall events into distinct  
 291 episodes based on soil depth and in rain saturated hydraulic conductivity (Fig. 10a). Using these episodes as the  
 292 basic analytical units, we then assess the intensity of slope-surface responses and the associated water distribution.  
 293 This approach overcomes the limitations of using rainfall statistics alone. It explicitly addresses the slope's dynamic  
 294 absorption-response behavior and shifts the focus from single-storm triggering to a more comprehensive assessment  
 295 of cumulative rainfall-response lags.



296  
297  
298  
299

**Figure 10.** Analysis of rainfall, soil moisture, and their coupling from 22 May to 7 July 2023. **(a)** Classification of rainfall episodes by vegetation type; **(b)** Temporal variation in volumetric soil water content for woodland and shrubland; **(c)** C Coupling between rainfall input and soil-moisture response for woodland and shrubland.

300  
301  
302  
303  
304  
305

From 22 May to 7 July 2023, volumetric water content indicates that shrubland soils beneath the sliding layer (layer 3) are insensitive to rainfall and show only small variations in water content (Fig. 10b). This is consistent with the findings in Sect. 4.2. In shrubland, most water remains near the surface, and infiltration capacity is low. To characterize the rainfall-soil-water coupling process, we introduce the index  $R_C$ , which quantifies how efficiently rainfall is converted into soil-water storage (Fig. 10c). A steeper slope in the regression of  $R_C$  versus soil water storage indicates a stronger soil-moisture response to rainfall.

306  
307  
308  
309  
310  
311  
312  
313  
314

In woodland,  $R_C$  values are generally positive, indicating that increases in soil-water content often exceed local rainfall input. Woodland soils have better-developed preferential flow paths than shrubland soils. This suggests that the observed excess arises because water infiltrating into upslope soils moves downslope as subsurface flow. This interpretation is consistent with the dye-tracer experiments. In woodland, foot-slope profiles show greater staining depths than upslope profiles (Fig. 8a). By contrast, early shallow saturation in shrubland diverts part of the rainfall input into overland flow, reducing conversion efficiency and yielding mostly negative  $R_C$  values. Overall, high  $R_C$  values in woodland reflect a strong hydrological response to rainfall and a greater capacity to buffer soil moisture. In shrubland, a pronounced response lag and low conversion efficiency lead to negative  $R_C$  values. These patterns are consistent with the earlier mechanism-based interpretation.

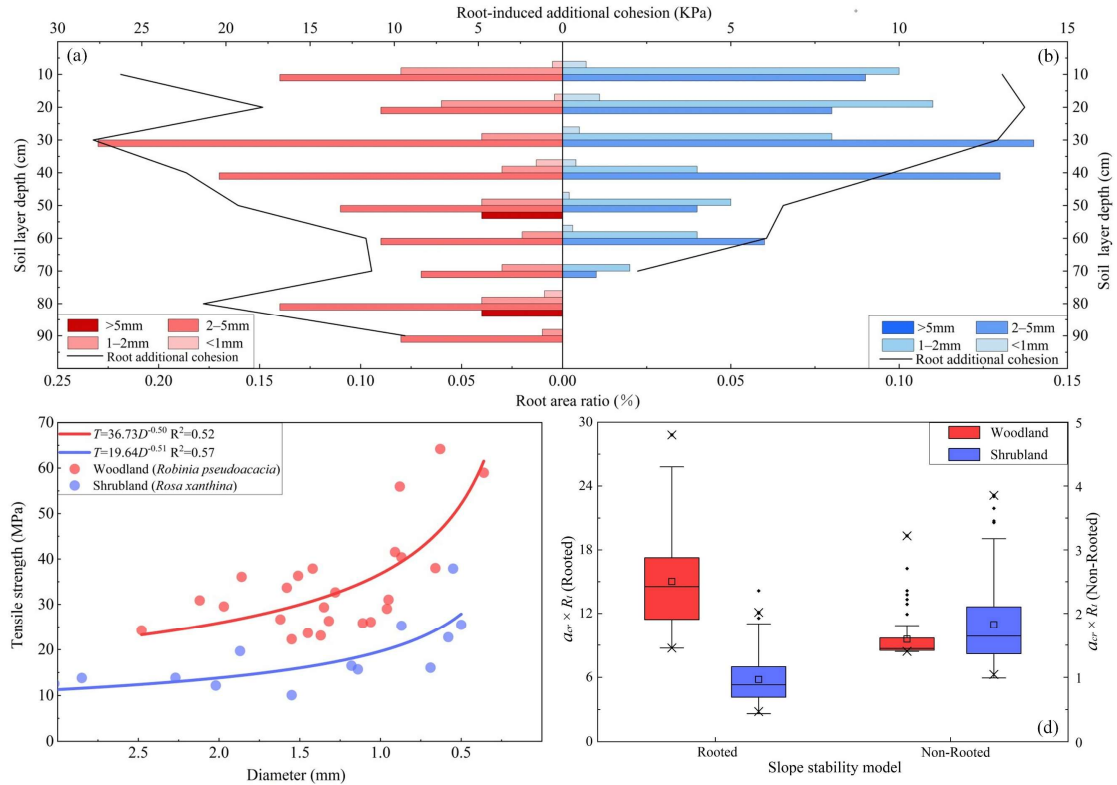
315

#### 4.4 Effects of vegetation roots on hillslope stability

316  
317  
318  
319  
320

Root spatial distribution and mechanical properties differ markedly between woodland and shrubland soils (Figs. 11a, 11b, and 11c). Field measurements indicate that maximum rooting depths in *Robinia pseudoacacia* and *Rosa xanthina* are close to their respective mean landslide depths, at 0.84 m in *Robinia pseudoacacia* and 0.54 m in *Rosa xanthina*. This consistency indicates a close relationship between root distribution and landslide depth. Compared with *Rosa xanthina*, roots in *Robinia pseudoacacia* mobilize greater root-induced cohesion at a given

321 root diameter and exhibit a larger specific root area ratio ( $RAR$ ). These roots therefore create a more extensive root-  
 322 soil contact interface and form a mechanically stronger root-soil composite.



323 **Figure 11.** Mechanical indices of slope stability in woodland and shrubland. **(a)** Root area ratio and root-induced  
 324 cohesion in woodland (*Robinia pseudoacacia*); **(b)** Root area ratio and root-induced cohesion in shrubland (*Rosa*  
 325 *xanthina*); **(c)** Relationship between root tensile strength and diameter; **(d)** Slope-stability models for woodland and  
 326 shrubland. The definitions of the boxplots is given in the caption of Fig. 5.  
 327

328 Using the parameters in Table 2, we constructed a slope stability model to evaluate slope resistance to failure  
 329 under specified topographic conditions and rainfall inputs. When root-induced cohesion is ignored, mean  $a_{rc} \times R_t$   
 330 values in woodland and shrubland are similar, indicating that slope stability differs little between them. When root  
 331 effects are included, slope stability increases markedly. In woodland, the  $a_{rc} \times R_t$  value rises to 15.02,  
 332 approximately 338% higher than in shrubland (Fig. 11d). These results indicate that woodland roots contribute much  
 333 more to slope stability than roots in shrubland. Woodland roots substantially increase the critical rainfall and  
 334 topographic thresholds for landslide initiation and confirm the key role of roots in strengthening slopes and resisting  
 335 landslide-triggering factors.

336 **Table 2** Parameters describing the slope stability model

Parameters	Definition	Woodland	Shrubland
$\rho_s$ ( $\text{kg}\cdot\text{m}^{-3}$ )	Dry soil density	1.37	1.41
$\theta$ ( $^\circ$ )	Slope gradient	31.71–65.27	22.78–67.96
$C'$ (kPa)	Effective soil cohesion	5.97	7.35
$C_r$ (kPa)	Root-induced cohesion	18.59	10.36
$\varphi$ ( $^\circ$ )	Effective friction angle	18.67	14.50
$z$ (m)	Landslide depth	0.84	0.54
$K$ ( $\text{mm}\cdot\text{h}^{-1}$ )	Hydraulic conductivity	2.10	0.94

## 337 **5 Discussion**

338 Long-term vegetation restoration policies may result in the dominant soil erosion process shift from traditional  
339 wind and water erosion to landslides (Deng et al., 2022; Yang et al., 2024; Du et al., 2025; Liao et al., 2025).  
340 Ecological restoration forests not only increase surface cover, but the recovered vegetation extends their root systems  
341 into potential sliding layers, thereby substantially altering slope hydrological processes and mechanical properties,  
342 and playing an important role in landslide initiation (Zhao et al., 2022; Cai et al., 2024; Chen et al., 2024; Lann et  
343 al., 2024). In this context, our results highlight the hydro-mechanical heterogeneity across the *Robinia*  
344 *pseudoacacia*-dominated woodland and *Rosa xanthina*-dominated shrubland, and assessed its influence on  
345 landslide initiation.

346 The results of SWCC and HCF agree well with the infiltration patterns observed in dye-tracer experiments. In  
347 woodland soils, continuous preferential flow channels promote rapid infiltration, substantial downward water  
348 migration, and a high capacity for water storage and drainage. Shrubland soils exhibit scattered preferential flow  
349 channels, shorter infiltration pathways, pronounced shallow saturation, and a weaker capacity for water  
350 redistribution. The stained area ratio and patch distribution further corroborate these differences. Woodland profiles  
351 display vertical and continuous stained bands with greater infiltration depths, whereas shrubland profiles show  
352 shallow staining. This comparison indicates that variations in root distribution and diameter modify soil pore  
353 structure and thereby affect infiltration (Guan et al., 2024; Lann et al., 2024). Woodland soil with coarse roots and  
354 higher porosity facilitate deeper infiltration, whereas shrubland soils with shallow root systems provide lower  
355 infiltration capacity (Souza et al., 2023; Xiao et al., 2024; Hu et al., 2025). Preferential flow may result in the excess  
356 soil water storage over the rainfall depth, and the results from monitoring multiple natural rainfall events between  
357 20 May and 6 July 2023 further corroborate the assumption. In shrubland, soil moisture typically exhibits a delayed  
358 and attenuated response to rainfall.  $R_C$  values are consistently below zero, indicating low rainfall conversion  
359 efficiency. Most rainwater does not infiltrate but instead runs off once shallow soils saturate rapidly. In contrast,  
360 once rainfall over woodland slopes reaches a certain intensity,  $R_C$  values become positive. This pattern suggests that  
361 woodland slopes effectively intercept and infiltrate rainfall, sustain deeper water storage, and delay the development  
362 of saturation zones. This discrepancy is also evident in the critical  $a_{cr} \times R_t$  values. The failure resistance on  
363 woodland slopes is higher than shrubland slopes, which may explain the contrasting distribution patterns observed  
364 in landslide number and size.

365 Vegetation-based slope protection has long been regarded as a key measure in traditional soil and water  
366 conservation, yet multidisciplinary studies have revealed its dual effects (Gyssels et al., 2005; Sidle and Bogaard,  
367 2016; Lann et al., 2024). Some herbaceous plants with shallow root systems can promote rapid surface saturation  
368 during intense rainfall, thereby enhancing hillslope runoff and rill erosion (Gong et al., 2024). Certain fast-growing  
369 tree species with shallow root systems may provide only limited soil reinforcement and thus increase the risk of  
370 shallow landslides (Ghestem and Sidle, 2011; Lin et al., 2024). Moreover, excessively thick litter layers can impede  
371 infiltration during short-duration storms and accelerate runoff concentration (Zhou et al., 2018; Rajão et al., 2023).  
372 These observations indicate that vegetation-based measures are not universally effective for soil erosion control  
373 (Löbmann et al., 2020; Lann et al., 2024). Our results further support this understanding. Shallow landslide initiation  
374 depends not only on rainfall but also on vegetation type, which modifies coupled hydrological-mechanical processes  
375 on slopes. The deep root systems and stable preferential flow channels in woodland slopes may provide greater  
376 resilience against slope failure compared to shrubland slopes. This finding provides empirical evidence for forest-  
377 type allocation in ecologically sensitive areas. It also highlights the need for appropriate vegetation-type selection  
378 and matching in regional soil and water conservation.

## 379 **6 Conclusions**

380 Vegetation recovery on the Chinese Loess Plateau has altered the dominant soil erosion process from runoff-  
381 driven erosion to gravity-driven mass movements. Though previous studies have extensively investigated vegetation  
382 effects on soil erosion, the specific role of vegetation in landslide initiation remains poorly understood. In this study,  
383 we systematically examined landslide initiation processes in two contrasting vegetated landscapes: *Robinia*  
384 *pseudoacacia*-dominated woodlands and *Rosa xanthina*-dominated shrublands, focusing on hydro-mechanical  
385 heterogeneity. Following results can be drawn:

386 1. Landslides in woodland and shrubland exhibit obvious differences in initiation, depth and number. Shrubland  
387 has a higher density of small, shallow landslides, whereas woodland has fewer but deeper and larger failures. This  
388 contrast reflects a high-initiation-threshold and deep-seated-failure regime in woodland.

389 2. In shrubland, a loose, discontinuous pore system and pronounced hysteresis concentrate moisture in shallow  
390 layers, causing rapid shallow saturation and large rainfall losses. In woodland, stable preferential flow paths promote  
391 deeper and more efficient moisture migration, as reflected in higher soil water response index.

392 3. Woodland roots extend deeper and span a wider depth range than shrubland roots. Within the same depth  
393 interval, root additional cohesion and *RAR* are also higher than those in shrubland. These patterns indicate stronger  
394 root-network reinforcement in woodland soils and lower susceptibility to shallow landslides than in shrubland.  
395 Therefore, the sediment production from landslide erosion may differ in various forest types, which has been rarely  
396 addressed and deserves further study in future.

## 397 **Acknowledgments**

398 This research has been supported by the State Key Program of Natural Science of China (grant no. 42130701), and  
399 the Natural Science Foundation of China (grant no. 42177309). The authors extend their gratitude to personnel at  
400 the Jixian National Ecosystem Research Station of Shanxi Province, Beijing Forestry University, for their help during  
401 field investigations.

## 402 **Code and data availability**

403 The corresponding author, Prof. Chao Ma, is willing to share the raw/processed data upon reasonable request.

## 404 **Author contributions**

405 **Prof. Ma** conceived the study based on his expertise in shallow landslides and unsaturated soil mechanics, and  
406 proposed the concept of hydrological and hydromechanical coupling for analyzing vegetation-related slope  
407 instability. Under the guidance of Prof. Ma, **Ruijie Yang** conducted soil hydrology experiments and drafted the  
408 manuscript. **Xi Yang and Xinying Wang** assisted with field investigations. **Yan Zang and Liquan Lyu** contributed  
409 research progress on shallow landslides and vegetation–slope interactions in the study area.

## 410 **Competing interests**

411 The authors declare no conflicts of interest.

## 412 **References**

- 413 An, J., Gao, G., Yuan, C., and Fu, B.: Inter- and intra-event rainfall partitioning dynamics of two typical xerophytic  
414 shrubs in the loess plateau of china, *Hydrology and Earth System Sciences Discussions*, 26, 3885-3900,  
415 <https://doi.org/10.5194/hess-26-3885-2022>, 2022.
- 416 Bachmair, S., Weiler, M., and Troch, P. A.: Intercomparing hillslope hydrological dynamics: spatio-temporal

417 variability and vegetation cover effects, *Water Resour. Res.*, 48, W5537, <https://doi.org/10.1029/2011WR011196>,  
418 2012.

419 Bai, R., Wang, X., Li, J., Yang, F., Shangguan, Z., and Deng, L.: The impact of vegetation reconstruction on soil  
420 erosion in the loess plateau, *J. Environ. Manage.*, 363, 121382, <https://doi.org/10.1016/j.jenvman.2024.121382>,  
421 2024.

422 Borrelli, P., Robinson, D. A., Panagos, P., Lugato, E., Yang, J. E., Alewell, C., Wuepper, D., Montanarella, L., and  
423 Ballabio, C.: Land use and climate change impacts on global soil erosion by water (2015-2070), *Proc. Natl. Acad.*  
424 *Sci. U. S. A.*, 117, 21994-22001, <https://doi.org/10.1073/pnas.2001403117>, 2020.

425 Cai, L., Wang, F., Lin, Y., Long, Q., Zhao, Y., Han, J., Ge, W., and Chen, H.: Changes in preferential flow caused  
426 by root effects in black locust plantations of different stand ages in the semi-arid region of the loess plateau, *J.*  
427 *Hydrol.*, 634, 131086, <https://doi.org/10.1016/j.jhydrol.2024.131086>, 2024.

428 Chen, M., Yang, X., Zhang, X., Bai, Y., Shao, M., Wei, X., Jia, Y., Wang, Y., Jia, X., Zhu, Y., Zhang, Q., Zhu, X.,  
429 and Li, T.: Response of soil water to long-term revegetation, topography, and precipitation on the chinese loess  
430 plateau, *Catena*, 236, 107711, <https://doi.org/10.1016/j.catena.2023.107711>, 2024.

431 Deng, J., Ma, C., and Zhang, Y.: Shallow landslide characteristics and its response to vegetation by example of july  
432 2013, extreme rainstorm, central loess plateau, china, *Bull. Eng. Geol. Environ.*, 81, 100, <https://doi.org/10.1007/s10064-022-02606-1>, 2022.

434 Dibiagio, A., Capobianco, V., Oen, A., and Tallaksen, L. M.: State-of-the-art: parametrization of hydrological and  
435 mechanical reinforcement effects of vegetation in slope stability models for shallow landslides, *Landslides*, 21,  
436 2417-2446, <https://doi.org/10.1007/s10346-024-02300-1>, 2024.

437 Du, P., Chen, Y., Zhao, Y., Qu, L., Liu, H., Liu, Z., Xu, J., and Tian, X.: Formation process and depositional  
438 characteristics of mudballs in the loess plateau during extreme rainstorms: dual-threshold constraints on material  
439 sources and dynamic conditions, *J. Environ. Manage.*, 391, 126590, [https://doi.org/10.1016/j.jenvman.2025.](https://doi.org/10.1016/j.jenvman.2025.126590)  
440 126590, 2025.

441 Fan, L., Lehmann, P., Zheng, C., and Or, D.: Rainfall intensity temporal patterns affect shallow landslide triggering  
442 and hazard evolution, *Geophys. Res. Lett.*, 47, e2019GL085994, [https://doi.org/https://doi.org/10.1029/2019GL](https://doi.org/https://doi.org/10.1029/2019GL085994)  
443 085994, 2020.

444 Feng, X., Fu, B., Piao, S., Wang, S., Ciais, P., Zeng, Z., Lü, Y., Zeng, Y., Li, Y., Jiang, X., and Wu, B.: Revegetation  
445 in china's loess plateau is approaching sustainable water resource limits, *Nat. Clim. Chang.*, 6, 1019-1022,  
446 <https://doi.org/10.1038/nclimate3092>, 2016.

447 Franklin, S. M., Kravchenko, A. N., Vargas, R., Vasilas, B., Fuhrmann, J. J., and Jin, Y.: The unexplored role of  
448 preferential flow in soil carbon dynamics, *Soil Biology and Biochemistry*, 161, 108398, [https://doi.org/10.1016/](https://doi.org/10.1016/j.soilbio.2021.108398)  
449 [j.soilbio.2021.108398](https://doi.org/10.1016/j.soilbio.2021.108398), 2021.

450 Fu, B., Wang, S., Liu, Y., Liu, J., Liang, W., and Miao, C.: Hydrogeomorphic ecosystem responses to natural and  
451 anthropogenic changes in the loess plateau of china, *Annual Review of Earth & Planetary Sciences*, 45, 223-243,  
452 <https://doi.org/10.1146/annurev-earth-063016-020552>, 2016.

453 Ghestem, M. and Sidle, R.: The influence of plant root systems on subsurface flow: implications for slope stability,  
454 *Bioscience*, 61, 869-879, <https://doi.org/10.1525/bio.2011.61.11.6>, 2011.

455 Gong, C., Ni, D., Liu, Y., Li, Y., Huang, Q., Tian, Y., and Zhang, H.: Herbaceous vegetation in slope stabilization:  
456 a comparative review of mechanisms, advantages, and practical applications, *Sustainability*, 16, 7620,  
457 <https://doi.org/10.3390/su16177620>, 2024.

458 Gu, C., Mu, X., Gao, P., Zhao, G., Sun, W., Tatarko, J., and Tan, X.: Influence of vegetation restoration on soil  
459 physical properties in the loess plateau, china, *J. Soils Sediments*, 19, 716-728, <https://doi.org/10.1007/s11368->

460 018-2083-3, 2019.

461 Guan, N., Bi, H., Song, Y., Lu, S., Lin, D., and Han, J.: Vegetation restoration is affecting the characteristics and  
462 patterns of infiltration in the loess plateau, *Catena*, 243, 108190, <https://doi.org/10.1016/j.catena.2024.108190>,  
463 2024.

464 Gyssels, G., Poesen, J., Bochet, E., and Li, Y.: Impact of plant roots on the resistance of soils to erosion by water: a  
465 review, *Progress in Physical Geography*, 29, 189-217, <https://doi.org/10.1191/0309133305pp443ra>, 2005.

466 Hao, M., Jin, Z., Luo, D., Cao, G., Jiang, C., Han, H., Yang, S., and Zhang, J.: Rainstorm erosion difference and  
467 topographical changes induced by heavy rainfall between afforestation and grassland restoration catchments on  
468 the chinese loess plateau, *Geomorphology*, 457, 109243, <https://doi.org/10.1016/j.geomorph.2024.109243>, 2024.

469 Hu, J., Ren, Y., Tang, M., Zhang, Z., Yang, K., Zhen, Q., and Han, F.: Effects of vegetation restoration on infiltration  
470 patterns and preferential flow in semi-arid areas with shallowly buried soft bedrock (pisha sandstone) in china, *J.*  
471 *Hydrol.*, 661, 133546, <https://doi.org/10.1016/j.jhydrol.2025.133546>, 2025.

472 Lan, H., Zhao, X., Macciotta, R., Peng, J., Li, L., Wu, Y., Zhu, Y., Liu, X., Zhang, N., and Liu, S.: The cyclic  
473 expansion and contraction characteristics of a loess slope and implications for slope stability., *Sci. Rep.*, 11, 2250,  
474 <https://doi.org/10.1038/s41598-021-81821-4>, 2021.

475 Lann, T., Bao, H., Lan, H., Zheng, H., Yan, C., and Peng, J.: Hydro-mechanical effects of vegetation on slope  
476 stability: a review, *Sci. Total Environ.*, 926, 171691, <https://doi.org/10.1016/j.scitotenv.2024.171691>, 2024.

477 Laycock, W. A., Geological Survey U. S., I. B., New, J. D. O. W., United, S. F. S., and Rutgers, U. (Eds.):  
478 Distribution of roots and rhizomes in different soil types in the pine barrens of new jersey, U.S. Geological Survey  
479 Professional Paper, Washington, 1967.

480 Li, F., Song, X., Tang, C., Liu, C., Yu, J., and Zhang, W.: Tracing infiltration and recharge using stable isotope in  
481 taihang mt., North china, *Environmental Geology*, 53, 687-696, <https://doi.org/10.1007/s00254-007-0683-0>, 2007.

482 Li, J., Cui, P., and Yin, Y.: Field observation and micro-mechanism of roots-induced preferential flow by infiltration  
483 experiment and phase-field method, *J. Hydrol.*, 623, 129756, <https://doi.org/10.1016/j.jhydrol.2023.129756>, 2023.

484 Li, P., Pan, Z., Xiao, T., and Wang, J.: Effects of molding water content and compaction degree on the microstructure  
485 and permeability of compacted loess, *Acta Geotech.*, 18, 921-936, <https://doi.org/10.1007/s11440-022-01592-8>,  
486 2023.

487 Li, S., Zheng, C., Lu, T., Zhou, K., Gu, Y., Wang, B., and Lu, Y.: Characteristics and influencing factors of loess  
488 terraces' preferential flow under different typical vegetation cover, *Plant Soil*, in press, <https://doi.org/10.1007/s11104-025-07710-1>, 2025.

490 Liang, H., Li, Y., An, X., Liu, J., Pan, N., and Li, Z.: Soil moisture dynamics and its temporal stability under  
491 different-aged caragana korshinskii shrubs in the loess hilly region of china, *Water*, 15, 2334, <https://doi.org/10.3390/w15132334>, 2023.

493 Liao, J., Wang, J., Jiao, J., Yan, Z., Li, J., Zhang, Z., Li, M., Xu, Q., Jiang, X., Zhao, W., Ling, Q., Sheng, H., Chen,  
494 Y., and Wu, T.: Rusle tends to overestimate soil erosion in revegetated conditions: evidence from long-term runoff  
495 plots monitoring on china's loess plateau, *Catena*, 258, 109285, <https://doi.org/10.1016/j.catena.2025.109285>,  
496 2025.

497 Lin, Y., Jian, W., Wu, Y., Zhu, Z., Wang, H., Dou, H., and Lai, Z.: Effect of tree roots on heavy rainfall-induced  
498 shallow landslides, *Geomatics, Natural Hazards and Risk*, 15, 2360002, <https://doi.org/10.1080/19475705.2024.2360002>, 2024.

500 Liu, X., Feng, T., Zhang, Y., Liu, Y., and Wang, P.: Vegetation restoration affects soil hydrological processes in  
501 typical natural and planted forests on the loess plateau, *J. Hydrol.*, 650, 132465, <https://doi.org/10.1016/j.jhydrol.2024.132465>, 2025.

503 Löbmann, M. T., Geitner, C., Wellstein, C., and Zerbe, S.: The influence of herbaceous vegetation on slope stability  
504 – a review, *Earth-Sci. Rev.*, 209, 103328, <https://doi.org/10.1016/j.earscirev.2020.103328>, 2020.

505 Lu, N. and Godt, J. W. (Eds.): *Hillslope hydrology and stability*, Cambridge University Press, Cambridge, U.K.,  
506 2013.

507 Lu, N., Calderon, A. R. A., Wayllace, A., Lovekin, J., and Crandall, A.: Suction stress–based rainfall intensity–  
508 duration method for slope instability prediction, *J. Geotech. Geoenviron. Eng.*, 150, 4024069, <https://doi.org/10.1061/JGGEFK.GTENG-12597>, 2024.

510 Masi, E. B., Tofani, V., Rossi, G., Cuomo, S., Wu, W., Salciarini, D., Caporali, E., and Catani, F.: Effects of roots  
511 cohesion on regional distributed slope stability modelling, *Catena*, 222, 106853, <https://doi.org/10.1016/j.catena.2022.106853>, 2023.

513 Montgomery, D. R. and Dietrich, W. E.: A physically based model for the topographic control on shallow landsliding,  
514 *Water Resour. Res.*, 30, 1153-1171, <https://doi.org/10.1029/93WR02979>, 1994.

515 Montgomery, D. R. and Dietrich, W. E.: Landscape dissection and drainage area-slope thresholds, in: *Process  
516 Models and Theoretical Geomorphology*, edited, John Wiley & Sons, Chichester, 221-246, 1994.

517 Montgomery, D. R., Schmidt, K. M., Greenberg, H. M., and Dietrich, W. E.: Forest clearing and regional landsliding,  
518 *Geology*, 28, 311-314, [https://doi.org/10.1130/0091-7613\(2000\)28<311:FCARL>2.0.CO;2](https://doi.org/10.1130/0091-7613(2000)28<311:FCARL>2.0.CO;2), 2000.

519 Nimmo, J. R., Perkins, K. S., Schmidt, K. M., Miller, D. M., Stock, J. D., and Singha, K.: Hydrologic characterization  
520 of desert soils with varying degrees of pedogenesis: 1. Field experiments evaluating plant-relevant soil water  
521 behavior, *Vadose Zone J.*, 8, 480-495, <https://doi.org/10.2136/vzj2008.0052>, 2009.

522 Niu, F., Pan, C., and Cui, Y.: Experimental investigation to the effect of different land-use on rainfall infiltration  
523 runoff patterns and preferential flow distribution in the loess area of western shanxi province, *Acta Ecologica  
524 Sinica*, 43, 4144-4166, <https://doi.org/10.5846/stxb202204130989>, 2023.

525 Rajão, P., Berg, M., Cornelissen, J., and Dias, A.: The effects of leaf traits on litter rainfall interception with  
526 consequences for runoff and soil conservation, *J. Ecol.*, 111, 2662-2675, <https://doi.org/10.1111/1365-2745.14203>,  
527 2023.

528 Schwarz, M., Preti, F., Giadrossich, F., Lehmann, P., and Or, D.: Quantifying the role of vegetation in slope stability:  
529 a case study in tuscany (italy), *Ecol. Eng.*, 36, 285-291, <https://doi.org/10.1016/j.ecoleng.2009.06.014>, 2010.

530 Sidle, R. C. and Bogaard, T. A.: Dynamic earth system and ecological controls of rainfall-initiated landslides, *Earth-  
531 Sci. Rev.*, 159, 275-291, <https://doi.org/10.1016/j.earscirev.2016.05.013>, 2016.

532 Souza, L. F. T., Hirmas, D. R., Sullivan, P. L., Reuman, D. C., Kirk, M. F., Li, L., Ajami, H., Wen, H., Sarto, M. V.  
533 M., Loecke, T. D., Rudick, A. K., Rice, C. W., and Billings, S. A.: Root distributions, precipitation, and soil  
534 structure converge to govern soil organic carbon depth distributions, *Geoderma*, 437, 116569,  
535 <https://doi.org/10.1016/j.geoderma.2023.116569>, 2023.

536 Tang, B., Jiao, J., Zhang, Y., Chen, Y., Wang, N., and Bai, L.: The magnitude of soil erosion on hillslopes with  
537 different land use patterns under an extreme rainstorm on the northern loess plateau, china, *Soil and Tillage  
538 Research*, 204, 104716, <https://doi.org/10.1016/j.still.2020.104716>, 2020.

539 Tang, P., Zhang, J., Li, Y., Wei, G., Hu, Y., and Zhao, J.: Effects of extreme rainfall on the morphological  
540 characteristics and spatial distribution of shallow landslides under different land use patterns in the loess region of  
541 western shanxi province, northern china, *Journal of Beijing Forestry University*, 45, 109-117, <https://doi.org/10.12171/j.1000-1522.20230070>, 2023.

543 Wang, N. and Zhang, T.: Soil pore structure and its research methods: a review, *Soil Water Res.*, 19, 1-24,  
544 <https://doi.org/10.17221/64/2023-SWR>, 2024.

545 Wang, R., Dong, Z., Zhou, Z., Wang, N., Xue, Z., and Cao, L.: Effect of vegetation patchiness on the subsurface

546 water distribution in abandoned farmland of the loess plateau, china, *Sci. Total Environ.*, 746, 141416,  
547 <https://doi.org/10.1016/j.scitotenv.2020.141416>, 2020.

548 Wang, R., Dong, Z., Zhou, Z., and Wang, P.: Temporal variation in preferential water flow during natural vegetation  
549 restoration on abandoned farmland in the loess plateau of china, *Land*, 8, 186, [https://doi.org/](https://doi.org/10.3390/land8120186)  
550 10.3390/land8120186, 2019.

551 Wang, X., Ma, C., Lyu, L., and Zhang, Y.: Erosion characteristics of shallow landslides under various land-use  
552 conditions: an example of the caijiachuan landslide, *Arid Zone Research*, 41, 697-705,  
553 <https://doi.org/10.13866/j.azr.2024.04.15>., 2024.

554 Wang, Y., Dong, G., Qu, L., Wu, Z., Zhao, F., and Shao, C.: Ecosystem functioning of the loess plateau in china  
555 from vegetation restoration relied largely on climate, *Forests*, 14, 27, <https://doi.org/10.3390/f14010027>, 2022.

556 Wei, Y. Z., Yao, Z. H., Chong, X. L., Zhang, J. H., and Zhang, J.: Microstructure of unsaturated loess and its  
557 influence on strength characteristics, *Sci. Rep.*, 12, 1502, <https://doi.org/10.1038/s41598-022-05464-9>, 2022.

558 Wen, S., Shao, M., and Wang, J.: Earthworm burrowing activity and its effects on soil hydraulic properties under  
559 different soil moisture conditions from the loess plateau, china, *Sustainability*, 12, 9303, [https://doi.org/](https://doi.org/10.3390/su12219303)  
560 10.3390/su12219303, 2020.

561 Xiao, T., Li, P., Fei, W., and Wang, J.: Effects of vegetation roots on the structure and hydraulic properties of soils:  
562 a perspective review, *Sci. Total Environ.*, 906, 167524, <https://doi.org/10.1016/j.scitotenv.2023.167524>, 2024.

563 Xu, P., Zhang, Q., Qian, H., Li, M., and Yang, F.: An investigation into the relationship between saturated  
564 permeability and microstructure of remolded loess: a case study from chinese loess plateau, *Geoderma*, 382,  
565 114774, <https://doi.org/10.1016/j.geoderma.2020.114774>, 2021.

566 Yamase, K., Ikeno, H., Hotta, N., Imawaka, M., Ohashi, M., Tanikawa, T., Todo, C., Dannoura, M., and Hirano, Y.:  
567 Effect of sprouting and corresponding root distribution of the shrub species *Eurya japonica* on slope stability,  
568 *Catena*, 238, 107869, <https://doi.org/10.1016/j.catena.2024.107869>, 2024.

569 Yan, X., Nunes, J. P., Sun, J., Tang, D., Wen, Y., and Li, Z.: Restored vegetation dominates the decrease in surface  
570 and subsurface runoff on the loess plateau, *J. Hydrol.*, 640, 131730, <https://doi.org/10.1016/j.jhydrol.2024.131730>,  
571 2024.

572 Yang, B., Jiao, J., Ma, X., Zhao, W., Ling, Q., Zhang, X., Han, J., Du, P., Chen, Y., and Chen, H.: Distribution and  
573 formation of soil balls under heavy rainstorm conditions in the northern loess plateau, *J. Hydrol.*, 625, 130103,  
574 <https://doi.org/10.1016/j.jhydrol.2023.130103>, 2023.

575 Yang, B., Ma, X., Jiao, J., Zhao, W., Ling, Q., Li, J., and Zhang, X.: Magnitude and hotspots of soil erosion types  
576 during heavy rainstorm events on the loess plateau: implications for watershed management, *Catena*, 246, 108365,  
577 <https://doi.org/10.1016/j.catena.2024.108365>, 2024.

578 Zhang, S., Liu, Y., Yang, M., Tian, P., Mu, X., and Zhao, G.: Impact of vegetation restoration on preferential flow  
579 and soil infiltration capacity in the hilly region of the loess plateau, *Journal of Hydrology: Regional Studies*, 59,  
580 102333, <https://doi.org/10.1016/j.ejrh.2025.102333>, 2025.

581 Zhang, Y., Tang, Z., Zhang, J., Zhang, Z., and Zhang, M.: Visualizing preferential flow paths using dye tracer and  
582 species diversity theory methods to explore their correlation to soil properties with random forest algorithm, *J.*  
583 *Hydrol.*, 638, 131570, <https://doi.org/10.1016/j.jhydrol.2024.131570>, 2024.

584 Zhao, M., Li, D., Huang, Y., Deng, Y., Yang, G., Lei, T., and Huang, Y.: Soil matrix infiltration characteristics in  
585 differently aged eucalyptus plantations in a southern subtropical area in china, *Catena*, 217, 106490,  
586 <https://doi.org/10.1016/j.catena.2022.106490>, 2022.

587 Zhou, Q., Zhou, X., Luo, Y., and Cai, M.: The effects of litter layer and topsoil on surface runoff during simulated  
588 rainfall in guizhou province, china: a plot scale case study, *Water*, 10, 915, <https://doi.org/10.3390/w10070915>,

589 2018.  
590